



Meshless Local Petrov-galerkin Method for Elasto-static Analysis of Thick-walled Isotropic Laminated Cylinders

M. J. Mahmoodabadi^a, M. M. Sarfarazi^b, A. Bagheri^b, G. H. Baradaran^c

^a Department of Mechanical Engineering, Sirjan University of Technology, Sirjan, Iran.

^b Department of Mechanical Engineering, University of Guilan, Rasht, Iran.

^c Department of Mechanical Engineering, Shahid Bahonar University, Kerman, Iran.

PAPER INFO

Paper history:

Received 18 March 2014

Received in revised form 15 April 2014

Accepted 26 June 2014

Keywords:

Meshless Local Petrov-Galerkin (MLPG)

Moving Least Squares (MLS)

Material Discontinuity

Thick-Walled Laminated Cylinders

ABSTRACT

In this paper, one of the simplest and most regular members of the family of the Meshless Local Petrov-Galerkin (MLPG) methods; namely MLPG5, is applied to analyze the thick-walled isotropic laminated cylinders under elasto-static pressure. A novel simple technique is proposed to eliminate a very important difficulty of the meshless methods to deal with material discontinuities regarding to the high continuity of their shape functions. The Moving Least Squares (MLS) approximation is used for constructing the trial functions, and a simple Heaviside step function is chosen for the test function. The direct interpolation method is employed to impose the essential boundary conditions. Acceptable agreements with the analytical solutions and finite element method results are obtained specially at the material discontinuity boundaries, which suggest its application in other classes of problems.

doi: 10.5829/idosi.ije.2014.27.11b.11

1. INTRODUCTION¹

Compared to the traditional finite element methods (FEM), the meshless methods have received a lot of attention in the past two decades; due to their potential in eliminating the costly effort of the mesh generation. The Meshless Local Petrov-Galerkin (MLPG) approach is one of the most successful meshless methods presented by Atluri and Zhu in 1998 [1]. The main advantage of this method over the FEM is that it does not need any mesh, either for the interpolation of the solution variables or for the integration of the weak forms. In the recent years, researchers have applied this approach to solve various engineering problems. For instance, Chen and Raju coupled the finite element and meshless local Petrov-Galerkin methods to solve two-dimensional potential problems [2]. Xiao proposed the local heaviside weighted MLPG meshless method for two-dimensional solids using compactly supported

radial basis functions [3]. Qian et al. studied the static and dynamic deformations of thick functionally graded elastic plates by the MLPG approach [4]. Li et al. applied a locking-free MPLG formulation for thick and thin plates [5]. Ma utilized the MLPG technique for two-dimensional nonlinear water wave problems [6]. Sladek analyzed the stress of the anisotropic functionally graded materials by the MLPG method [7]. Ching used the MLPG method to analyze two dimensional functionally graded elastic solids under mechanical and thermal loads [8]. Batra et al. analyzed the micro electro-mechanic systems using the MLPG technique [9]. Sladek et al. solved the inverse heat conduction problems by meshless local Petrov-Galerkin approach [10]. Kaiyuan et al. proposed a simple and less-costly MLPG technique for the dynamic fracture problem [11]. Xiao et al. analyzed the thick plates by using a higher-order shear and normal deformable plate theory and MLPG method with radial basis functions [12]. Sladek et al. used MLPG method for Reissner-Mindlin plates under dynamic load [13]. Gilhooley et al. analyzed the thick functionally graded plates by using

*Corresponding Author's Email: mahmoodabadi@sirjantech.ac.ir (M.J. Mahmoodabadi)

higher-order shear and normal deformable plate theory and MLPG method with radial basis functions [14]. Liu and Tan applied meshless local Petrov–Galerkin approach for coupled radiative and conductive heat transfer [15]. Hu et al. proposed a meshless local Petrov–Galerkin approach for large deformation contact analysis of elastomers [16]. Li et al. solved mindlin shell problem by meshless local Petrov-Galerkin [17]. Wu and Tao proposed a meshless method based on the local weak-forms for steady-state heat conduction problems [18]. Gilhooley et al. studied two-dimensional stress of functionally graded solids using the MLPG method with radial basis functions [19]. Sladek et al. solved the inverse fracture problems in piezoelectric solids by local integral equation methods [20]. Li et al. studied the fracture of cracked two dimensional planar and axisymmetric problems of magneto–electro-elastic materials by the MLPG coupled with FEM [21]. Sladek et al. analyzed the fracture in continuously nonhomogeneous magneto-electro-elastic solids under a thermal load by the MLPG approach [22]. Vaghefi et al. analyzed three-dimensional static of thick functionally graded plates by the MLPG method [23]. Wen used meshless local Petrov–Galerkin method for wave propagation in three dimensional poroelastic solids [24]. Wu et al. proposed a stabilized MLPG method for steady state incompressible fluid flow simulation [25]. Rezaei Mojdehi et al. analyzed three dimensional static and dynamic of thick functionally graded plates by the MLPG method [26]. Xia et al. analyzed the elasto-plastic problem of the moderately thick plate using the meshless local Petrov–Galerkin technique [27]. Hosseini used the meshless local Petrov–Galerkin method for coupled thermoelasticity analysis of a functionally graded thick hollow cylinder [28]. Shibahara and Atluri applied the meshless local Petrov-Galerkin method for the analysis of heat conduction due to a moving heat source [29]. Mahmoodabadi et al. used the meshless local Petrov-Galerkin method for three dimensional steady-state heat conduction problems [30]. Najafi et al. studied meshless local Petrov–Galerkin method for higher Reynolds numbers fluid flow applications [31]. Nikfar and Mahmoodi applied the MLPG method for free convection of nanofluid in a cavity with wavy side walls [32]. Sladek et al. studied the bending of circular piezoelectric plates with functionally graded material properties by a MLPG method [33]. Arefmanesh utilized meshless numerical methods for analysis of the buoyancy-driven fluid flow and heat transfer in a square cavity with a wavy baffle [34].

In the MLPG method, the integrations of the weak forms are performed over local sub-domains, which overlap with each other. The trial functions and the test functions are chosen from totally different functional spaces. Furthermore, the physical size of the test and the trial domains are not necessary to be the same, which

makes the MLPG a very flexible approach. By selecting the different trial and test functions, the MLPG method could be classified into six different types, which are labeled as MLPG1, MLPG2, MLPG3, MLPG4, MLPG5, and MLPG6 [35]. Among them, the MLPG5 shows high robustness and accuracy for solving two-dimensional problems [35]. Furthermore, the MLPG5 (wherein the test function is the Heaviside step function over a local sub-domain centered at a node) would eliminate the necessity of the domain integration for the problems without any body-forces.

Complicated nature of the meshless trial functions makes the three-dimensional application numerically demanding; specially, when the background cells and the domain integration are involved. Hence, the MLPG5 method can be efficient in dealing with this difficulty. On the other hand, treatment of the material discontinuities is a well-known drawback of the meshless methods with an inherent higher-order continuous displacement field. In fact, because of the highly continuous trial function which is at least C^1 , it is difficult to simulate jumps in the strain field. There have been a lot of efforts devoted to solve this problem. Li et al. [36] have used MLPG2 at the material discontinuity boundary, with two sets of collocation nodes coincident at the interface of two bodies, but with different material properties. The MLS interpolation is carried out separately within each of the homogeneous domains, so that the domain of influence is truncated at the interface of the two bodies. Although their proposed technique is needless of any integration process, the method is as accurate as MLPG2 at the material boundaries, so the number of collocation nodes must be much bigger. Krongauz and Belytschko [37] introduced a “jump shape function” and a trial function with a pre-imposed discontinuity in the gradient of the function at the location of the material discontinuity in 2-D elasticity. However, this method requires interpolation in the curvilinear coordinates, which becomes very tedious in three dimensional applications. Cordes and Moran [38] also solved the problem in 2-D elasticity by using Lagrange’s multiplier. Their method required both domain and boundary integrations on the surface of the discontinuity, which needs a lot of computational efforts when the discontinuity has an arbitrary geometrical shape.

To overcome to this problem, in this paper, a special treatment is applied at the location of material discontinuities in order to solve such problems. This new technique considers the subdomain of a node locating on the material boundary as two parts; one residing in the inner layer and the other one residing in the outer layer. The elasto-static analysis of the thick-walled open-end one-layer and two-layer cylinders made of isotropic materials are presented. The obtained results compared with the FEM results and exact solutions of the problem are presented in the appendix.

2. THE MLS APPROXIMATION SCHEME

As mentioned earlier, in the MLPG method, the test and trial functions are not necessarily from the same space. Thus, we can choose the Moving Least Squares (MLS) interpolation as the trial function while employ the Heaviside step function as the test function over each local sub-domain.

The MLS method was presented by mathematicians for data fitting and surface construction. This method is generally considered to be one of the useful interpolation schemes that approximates random data with reasonable accuracy. It has two major features which have made it popular: (a) the approximated field function is continuous and smooth in the entire problem domain (what becomes a drawback at the material discontinuity boundaries); (b) it is capable of producing an approximation with the desired order of consistency. The MLS approximation of u for any point $\mathbf{x} \in \Omega_x$ (Figure 1) is defined by [1]:

$$u^h(\mathbf{x}) = \mathbf{p}^T(\mathbf{x})\mathbf{a}(\mathbf{x}) \quad \forall \mathbf{x} \in \Omega_x \quad (1)$$

where, Ω_x is a neighborhood area of point \mathbf{x} , and we call it the definition domain of point \mathbf{x} . $\mathbf{p}^T(\mathbf{x}) = [p_1(\mathbf{x}), p_2(\mathbf{x}), \dots, p_m(\mathbf{x})]$ is a monomial basis of order m . In the three dimensions problems, the linear basis is defined as:

$$\mathbf{p}^T(\mathbf{x}) = [1, x, y, z] \quad m = 4 \quad (2)$$

and the quadratic basis is defined as:

$$\mathbf{p}^T(\mathbf{x}) = [1, x, y, z, x^2, y^2, z^2, xy, yz, xz] \quad m = 10 \quad (3)$$

Also, $\mathbf{a}(\mathbf{x})$ is a vector containing coefficients which are functions of the global Cartesian coordinates $[x \ y \ z]$ depending on the monomial basis. $\mathbf{a}(\mathbf{x})$ is determined by minimizing a weighted discrete L_2 norm defined as:

$$J(\mathbf{a}(\mathbf{x})) = \sum_{I=1}^N w_I(\mathbf{x}) [\mathbf{p}^T(\mathbf{x}_I)\mathbf{a}(\mathbf{x}) - \hat{u}^I]^2 = [\mathbf{P}\mathbf{a}(\mathbf{x}) - \hat{\mathbf{u}}]^T \mathbf{W} [\mathbf{P}\mathbf{a}(\mathbf{x}) - \hat{\mathbf{u}}] \quad (4)$$

where, $w_I(\mathbf{x})$ is the weight function, and \hat{u}^I is the fictitious nodal value. \mathbf{P} , \mathbf{W} , and $\hat{\mathbf{u}}$ are identified as follows:

$$\mathbf{P} = \begin{bmatrix} \mathbf{p}^T(\mathbf{x}_1) \\ \mathbf{p}^T(\mathbf{x}_2) \\ \dots \\ \mathbf{p}^T(\mathbf{x}_N) \end{bmatrix}_{N \times m}, \quad \mathbf{W} = \begin{bmatrix} w_1(\mathbf{x}) & \dots & 0 \\ \vdots & \ddots & \vdots \\ 0 & \dots & w_N(\mathbf{x}) \end{bmatrix}_{N \times N}, \quad \hat{\mathbf{u}} = [\hat{u}^1, \hat{u}^2, \dots, \hat{u}^N]_{1 \times N} \quad (5)$$

The stationary of J in Equation (4) with respect to $\mathbf{a}(\mathbf{x})$ leads to following linear relation between $\mathbf{a}(\mathbf{x})$ and $\hat{\mathbf{u}}$,

$$\mathbf{A}(\mathbf{x})\mathbf{a}(\mathbf{x}) = \mathbf{B}(\mathbf{x})\hat{\mathbf{u}}, \quad \mathbf{A} : (m \times m); \mathbf{a} : (m \times 1); \mathbf{B} : (m \times N); \hat{\mathbf{u}} : (N \times 1) \quad (6)$$

where, matrices $\mathbf{A}(\mathbf{x})$ and $\mathbf{B}(\mathbf{x})$ are defined by:

$$\mathbf{A}(\mathbf{x}) = \mathbf{P}^T \mathbf{W} \mathbf{P}, \quad \mathbf{B}(\mathbf{x}) = \mathbf{P}^T \mathbf{W} \quad (7)$$

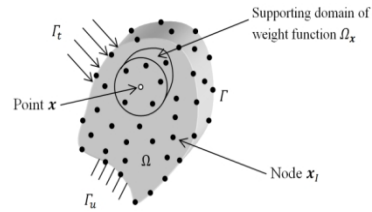


Figure 1. Schematics of the MLS approximation

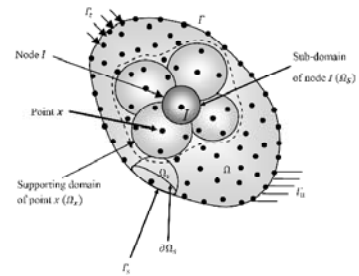


Figure 2. Different positions of the spherical sub-domain.

Once coefficients $\mathbf{a}(\mathbf{x})$ in Equation (6) are determined, one may obtain the approximation from the nodal values at the local scattered points, by substituting them into Equation (1), as:

$$u^h(\mathbf{x}) = \Phi^T(\mathbf{x}) \cdot \hat{\mathbf{u}} = \sum_{I=1}^N \phi^I(\mathbf{x}) \hat{u}^I \quad \text{and} \quad u^h(\mathbf{x}) \equiv u^I \neq \hat{u}^I \quad \forall \mathbf{x} \in \Omega_x \quad (8)$$

With

$$\Phi^T(\mathbf{x}) = \mathbf{p}^T(\mathbf{x})\mathbf{A}^{-1}(\mathbf{x})\mathbf{B}(\mathbf{x}), \quad \phi^I(\mathbf{x}) = \sum_{j=1}^m p_j(\mathbf{x}) [\mathbf{A}^{-1}(\mathbf{x})\mathbf{B}(\mathbf{x})]_{jI} \quad (9)$$

The weight function in Equation (4) defines the range of influence of node I . Normally, it has a compact support. In this article, a 4th order quadratic spline weight function is used.

$$w_I(\mathbf{x}) = \begin{cases} 1 - 6 \left(\frac{d_I}{r_I}\right)^2 + 8 \left(\frac{d_I}{r_I}\right)^3 - 3 \left(\frac{d_I}{r_I}\right)^4 & 0 \leq d_I \leq r_I \\ 0 & d_I \geq r_I \end{cases} \quad (10)$$

where, d_I is the distance between point \mathbf{x} and node \mathbf{x}_I , also r_I is the size of support for the weight functions. It can be seen that the quadratic spline weight function is C^1 continuous over the entire domain [1].

3. MLPG5 FORMULATION FOR THREE-DIMENSIONAL ELASTICITY AND NUMERICAL DISCRETIZATION

Despite the conventional Galerkin approaches such as element free Galerkin, which are based on global weak-form of the problem, the MLPG method constructs the weak-form over the local sub-domains like Ω_s [1]. As well, Ω_s is a small region taken for each node inside the global domain (Figure 2).

The equations of equilibrium in a volume Ω bounded by surface Γ , are given by [1]:

$$\sigma_{ij,j} + b_i = 0 \tag{11}$$

where, σ_{ij} is the stress tensor, b_i is the body force, and $()_{,i}$ means $\partial/(\partial x^i)$ (with $(x^1, x^2, x^3) \equiv (x, y, z)$). The boundary conditions are assumed as [1]:

$$t_i \equiv \sigma_{ij}n_j = \bar{t}_i \text{ on } \Gamma_t, \quad u_i = \bar{u}_i \text{ on } \Gamma_u \tag{12}$$

where, \bar{u}_i are the prescribed displacements, \bar{t}_i are the prescribed surface tractions, \mathbf{n} is the unit outward normal of the global boundary, Γ_u is the global boundary with prescribed displacements and Γ_t is the global boundary with prescribed surface tractions.

The local sub-domains could be of any geometric shape. However, in this paper, they are taken to be of spherical shape for simplicity. The local weak form of the equilibrium equations over the sub-domain around node I is given in Equation (13).

$$\int_{\Omega_s} (\sigma_{ij,j} + b_i)v_i d\Omega - \alpha \int_{\Gamma_{su}} (u_i - \bar{u}_i)v_i d\Gamma = 0 \tag{13}$$

where, v_i is the test function. The penalty parameter α is introduced in order to satisfy the essential boundary conditions. Using $\sigma_{ij,j}v_i = (\sigma_{ij}v_i)_{,j} - \sigma_{ij}v_{i,j}$ and the divergence theorem, we have:

$$\int_{\partial\Omega_s} \sigma_{ij}n_j v_i d\Gamma - \int_{\Omega_s} (\sigma_{ij}v_{i,j} - b_i v_i) d\Omega - \alpha \int_{\Gamma_{su}} (u_i - \bar{u}_i)v_i d\Gamma = 0 \tag{14}$$

By applying the natural boundary conditions ($t_i \equiv \sigma_{ij}n_j = \bar{t}_i$), we can obtain the local symmetric weak-form in linear elasticity which leads to MLPG1, MLPG5, and MLPG6 approaches.

$$\int_{\Omega_s} \sigma_{ij}v_{i,j} d\Omega - \int_{L_s} t_i v_i d\Gamma + \alpha \int_{\Gamma_{su}} u_i v_i d\Gamma - \int_{\Gamma_{st}} t_i v_i d\Gamma = \int_{\Gamma_{st}} \bar{t}_i v_i d\Gamma + \alpha \int_{\Gamma_{su}} \bar{u}_i v_i d\Gamma + \int_{\Omega_s} b_i v_i d\Omega \tag{15}$$

If a Heaviside step function is chosen as the test function in each sub-domain, we'll reach the MLPG5 method [35]. Hence, the above equation reduces to:

$$- \int_{L_s} t_i d\Gamma + \alpha \int_{\Gamma_{su}} u_i d\Gamma - \int_{\Gamma_{st}} t_i d\Gamma = \int_{\Gamma_{st}} \bar{t}_i d\Gamma + \alpha \int_{\Gamma_{su}} \bar{u}_i d\Gamma + \int_{\Omega_s} b_i d\Omega \tag{16}$$

It is seen that in Equation (16), there is no domain integration involved in the left hand side (leading to the stiffness matrix after discretization). Thus, if there were no body forces, the domain integration would be totally eliminated. One can discretize the MLPG5 by substituting the MLS interpolation function Equation (8) into Equation (16).

$$- \sum_{j=1}^M \int_{L_s} \mathbf{NDB}^j \hat{\mathbf{u}}^j d\Gamma + \alpha \sum_{j=1}^M \int_{\Gamma_{su}} \mathbf{S}\phi^j \hat{\mathbf{u}}^j d\Gamma - \sum_{j=1}^M \int_{\Gamma_{st}} \mathbf{NDB}^j \hat{\mathbf{u}}^j d\Gamma = \int_{\Gamma_{st}} \bar{\mathbf{t}} d\Gamma + \alpha \int_{\Gamma_{su}} \bar{\mathbf{S}}\mathbf{u} d\Gamma + \int_{\Omega_s} \mathbf{b} d\Omega \tag{17}$$

with the definition of:

$$N = \begin{bmatrix} n_1 & 0 & 0 & 0 & n_3 & n_2 \\ 0 & n_2 & 0 & n_3 & 0 & n_1 \\ 0 & 0 & n_3 & n_2 & n_1 & 0 \end{bmatrix},$$

$$\mathbf{S} = \begin{bmatrix} S_1 & 0 & 0 \\ 0 & S_2 & 0 \\ 0 & 0 & S_3 \end{bmatrix}, \quad S_i = \begin{cases} 1 & \text{if } u_i \text{ is prescribed on } \Gamma_{su} \\ 0 & \text{if } u_i \text{ isn't prescribed on } \Gamma_{su} \end{cases}$$

$$\mathbf{B}^j = \begin{bmatrix} \phi_{,1}^j & 0 & 0 \\ 0 & \phi_{,2}^j & 0 \\ 0 & 0 & \phi_{,3}^j \\ 0 & \phi_{,3}^j & \phi_{,2}^j \\ \phi_{,3}^j & 0 & \phi_{,1}^j \\ \phi_{,2}^j & \phi_{,1}^j & 0 \end{bmatrix}$$

$$\mathbf{D} = \frac{E}{(1+\nu)(1-2\nu)} \begin{bmatrix} 1-\nu & \nu & \nu & 0 & 0 & 0 \\ \nu & 1-\nu & \nu & 0 & 0 & 0 \\ \nu & \nu & 1-\nu & 0 & 0 & 0 \\ 0 & 0 & 0 & 0.5-\nu & 0 & 0 \\ 0 & 0 & 0 & 0 & 0.5-\nu & 0 \\ 0 & 0 & 0 & 0 & 0 & 0.5-\nu \end{bmatrix}$$

E and ν are the Young's module and Poisson's ratio, respectively.

Equation (17) can be shorted to:

$$\sum_{j=1}^M \mathbf{K}_{Ij} \hat{\mathbf{u}}^j = \mathbf{f}_I, \quad I = 1, 2, \dots, M \tag{18}$$

M is the total number of the nodes. It's notable that $\phi^j(\mathbf{x})$ vanishes for the nodes outside the local sub-domain Ω_s , so taking all the nodes into account for each sub-domain does not affect the local sense of the procedure. The nodal stiffness matrix and force vector would be:

$$\mathbf{K}_{Ij} = - \int_{L_s} \mathbf{NDB}^j d\Gamma + \alpha \int_{\Gamma_{su}} \mathbf{S}\phi^j d\Gamma - \int_{\Gamma_{st}} \mathbf{NDB}^j d\Gamma \tag{19}$$

$$\mathbf{f}_I = \int_{\Gamma_{st}} \bar{\mathbf{t}} d\Gamma + \alpha \int_{\Gamma_{su}} \bar{\mathbf{S}}\mathbf{u} d\Gamma + \int_{\Omega_s} \mathbf{b} d\Omega \tag{20}$$

If we want to enforce the essential boundary conditions via the direct interpolation method, after omitting the terms consisted α in the above equations, we should replace both sides of the Equations (19) and (20) for the nodes on the essential boundary [39].

$$\mathbf{u}^{hl} = \begin{Bmatrix} u_x^{hl} \\ u_y^{hl} \\ u_z^{hl} \end{Bmatrix} = \begin{bmatrix} \phi^1 & 0 & 0 & \dots & \phi^M & 0 & 0 \\ 0 & \phi^1 & 0 & \dots & 0 & \phi^M & 0 \\ 0 & 0 & \phi^1 & \dots & 0 & 0 & \phi^M \end{bmatrix} \begin{Bmatrix} \hat{u}_x^1 \\ \hat{u}_y^1 \\ \hat{u}_z^1 \\ \vdots \\ \hat{u}_x^M \\ \hat{u}_y^M \\ \hat{u}_z^M \end{Bmatrix} = \tag{21}$$

$$\Phi \mathbf{u} = \begin{Bmatrix} \bar{u}_x^I \\ \bar{u}_y^I \\ \bar{u}_z^I \end{Bmatrix}$$

It's obvious that for the nodes which are having only one or two displacement components being prescribed on the essential boundary, the respective equation(s) will be substituted in Equations (19) and (20). Direct interpolation technique is straightforward and was suggested to be applied in MLPG by Atluri et al. [35]. So, this very effective method has been used to enforce the essential boundary conditions.

4. TREATMENT OF MATERIAL DISCONTINUITIES

As mentioned before, the MLPG method has been naturally lead to continuous differentiable

approximations so that the partial derivatives of the approximation such as strains and stresses in elastic problems are smooth and don't require any post-processing. However, this high continuous nature also leads to difficulty when there is an imposed discontinuity in the derivatives; e.g. the natural discontinuity in strains when material discontinuities are present.

The new technique presented in this paper considers the subdomain of a node locating on the material boundary as two parts; one residing in the inner layer and the other one residing in the outer layer (Figure 3). After calculating the Gaussian integration points for each part, we would select the neighboring nodes of the first part Gaussian points only from the nodes of the inner layer and vice versa. In other words, for the nodes locating exactly on the material boundary, we simply define the support domain of each Gaussian point not a perfect sphere but just a part of it, while the subdomains of these nodes are the same as the other nodes'. It is noteworthy that the support domains for the other nodes' Gaussian points must not intersect the material boundary as well. Another note is that the material boundary nodes, themselves, are not taken into account as the neighboring nodes of any Gaussian point, although they are included into the solution (Equations 18 and 21) with their own subdomains.

5. ELASTO-STATIC ANALYSIS OF THICK-WALLED LAMINATED CYLINDERS

As mentioned before, the elasto-static analysis of thick-walled cylinders can be a proper experiment for three-dimensional application of MLPG5. Moreover, studying the laminated cylinders, made of isotropic materials, helps us to challenge the performance of the proposed technique in dealing with the material discontinuities. Hence, a typical two-layer cylinder fulfils this objective. Adding more layers to the problem needs to pursue a similar procedure.

5. 1. One-layer Cylinder We consider an open-end cylinder of length $L = 15$, internal radius $r_i = 2$ and thickness of $t = 4.5$ subjected to uniform internal pressure $p_i = 1$. This cylinder is made of an isotropic material with $E = 1$ and $\nu = 0.3$ [35]. The problem is solved for one-fourth of the cylinder, due to the symmetry in the load and geometry (Figure 4).

Since the cylinder is open-end, the lengthwise stress vanishes ($\sigma_z = 0$), and the lengthwise strain ($\epsilon_z = \frac{\partial u_z}{\partial z}$) has a constant value. Further, because of symmetry and absence of shear loads, the tangential displacement and all of the shear stresses are zero. Considering Appendix A, radial and hoop stresses as well as the radial and lengthwise displacements are as below:

$$\sigma_r = \frac{16 - \frac{676}{r^2}}{153}, \quad \sigma_\theta = \frac{16 + \frac{676}{r^2}}{153} \tag{22}$$

$$u_r = \frac{56r + \frac{4394}{r}}{765}, \quad u_z = -\frac{16}{255}Z \tag{23}$$

The three-dimensional node distribution of the MLPG5 model with 132 nodes, including 4 nodes in the radial, 3 nodes in the tangential and 11 nodes in the lengthwise direction is shown in Figure 5. As said before, as well as the exact solution, the results would be compared with those obtained from the solution of software ANSYS. Since this software renders the results only at the nodes, we had to define enough nodes on the comparison direction ($z = 7.5$ and $\theta = 45^\circ$). This means that the number of nodes in ANSYS solution is much more than the MLPG5, but solutions with less number of nodes, which are not cited here, also have the similar results. In other words, the FEM solution of this problem is converged. In this example, we have applied the 20-node SOLID95 element which, according to ANSYS's HELP is very efficient for curvilinear domains. There are 425 nodes and 64 elements as shown in Figures 6 and 7. In addition, the boundary conditions and the loading are the same as the MLPG5 solution.

The results show an acceptable agreement with the exact solution and the FEM result which suggests its application in other classes of problems. In Figures 8 to 10, the radial displacement, radial stress, and hoop stress diagrams are shown at $z = 7.5$ and $\theta = 45^\circ$. Furthermore, the lengthwise displacement diagram at $\theta = 45^\circ$ and $r = 4.25$ is illustrated in Figure 11. It could be seen that the FEM results are almost perfect and obviously better than the MLPG5 results.

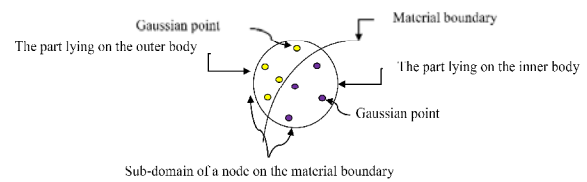


Figure 3. Segregation of the sub-domain respective to a node on the material boundary.

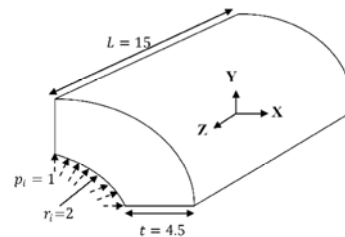


Figure 4. One-fourth of the one-layer cylinder subjected to internal pressure.

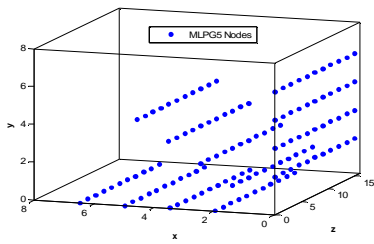


Figure 5. Three-dimensional node distribution of the MLPG5 model for one-fourth of the one-layer cylinder.

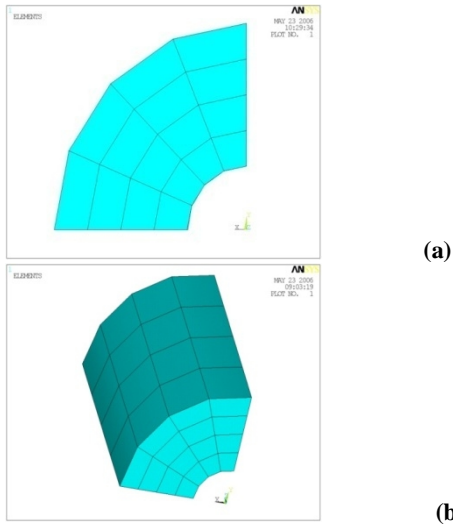


Figure 6. FEM model with 64 elements for one-fourth of the one-layer cylinder; a) a section parallel to X-Y plane, b) the isometric view.

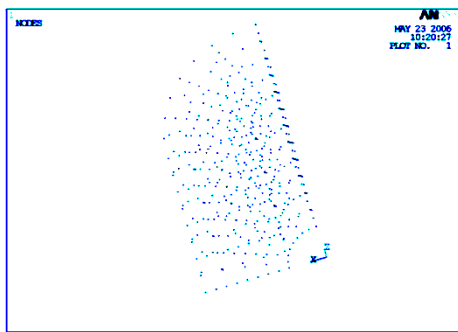


Figure 7. Isometric view of 425 nodes of the FEM model for one-fourth of the one-layer cylinder.

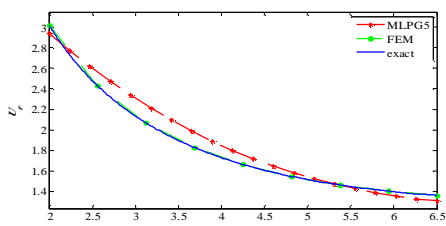


Figure 8. Radial displacement diagram at $z = 7.5$ and $\theta = 45^\circ$ for the one-layer cylinder.

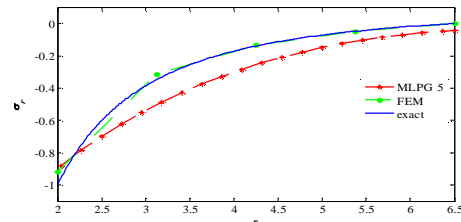


Figure 9. Radial stress diagram at $z = 7.5$ and $\theta = 45^\circ$ for the one-layer cylinder.

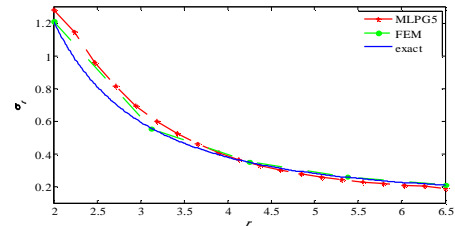


Figure 10. Hoop stress diagram at $z = 7.5$ and $\theta = 45^\circ$ for the one-layer cylinder.

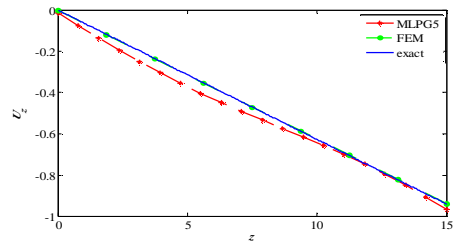


Figure 11. Lengthwise displacement diagram at $\theta = 45^\circ$ and $r = 4.25$ for the one-layer cylinder.

5. 2. Two-layer Cylinder An open-end two-layer cylinder of length $L = 30$ and internal radius $r_i = 2$ subjected to uniform internal pressure $p_i = 1$ is considered. The layers have the same thickness of $t_i = t_o = 3$ and the material properties are: $E_i = 1, \nu_i = 0.3, E_o = 2$ and $\nu_o = 0.25$ [35]. We assume that the layers are freely placed beside each other and have no deflection before being pressed by the internal pressure. Figure 12 shows a feature of one-fourth of the cylinder. The exact stress and displacement values are obtained referring to Appendix B (Equations (24) to (27)).

$$\sigma_r(Lay1) = \frac{-23 - \frac{33508}{r^2}}{8400}, \quad \sigma_r(Lay2) = \frac{541 - \frac{34624}{r^2}}{5200} \quad (24)$$

$$\sigma_\theta(Lay1) = \frac{-23 + \frac{33508}{r^2}}{8400}, \quad \sigma_\theta(Lay2) = \frac{541 + \frac{34624}{r^2}}{5200} \quad (25)$$

$$u_r(Lay1) = r \left(\frac{-23}{12000} + \frac{108901}{21000r^2} \right), \quad u_r(Lay2) = \frac{r}{2} \left(\frac{1623}{20800} + \frac{541}{65r^2} \right) \quad (26)$$

$$u_z(Lay1) = \frac{23}{14000}z, \quad u_z(Lay2) = -\frac{541}{20800}z \quad (27)$$

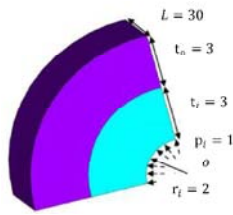


Figure 12. One-fourth of the two-layer cylinder subjected to internal pressure

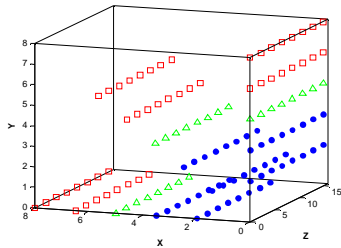


Figure 13. Three-dimensional node distribution of the MLPG5 model for one-fourth of the two-layer cylinder.

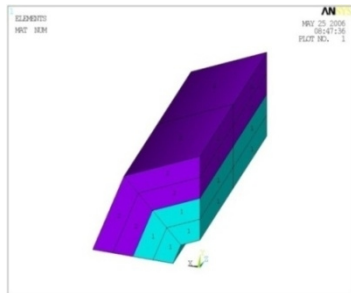


Figure 14. FEM model with 16 elements for one-fourth of the two-layer cylinder.

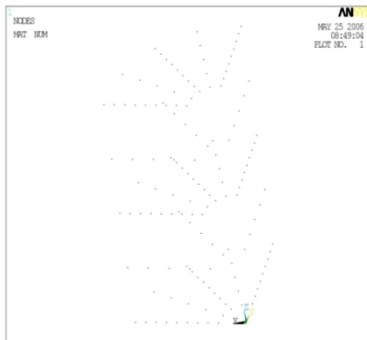


Figure 15. Isometric view of 164 nodes of the FEM model for one-fourth of the two-layer cylinder.

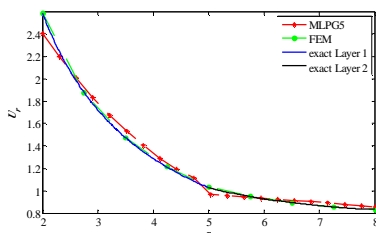


Figure 16. Radial displacement diagram at $z = 7.5$ and $\theta = 45^\circ$ for the two-layer cylinder.

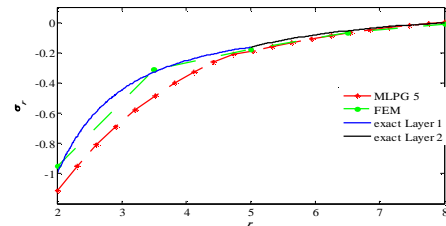


Figure 17. Radial stress diagram at $z = 7.5$ and $\theta = 45^\circ$ for the two-layer cylinder.

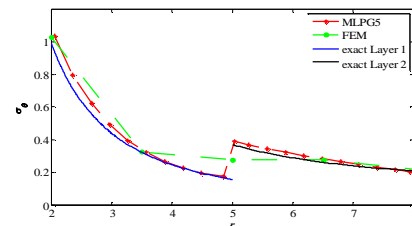


Figure 18. Hoop stress diagram at $z = 7.5$ and $\theta = 45^\circ$ for the two-layer cylinder.

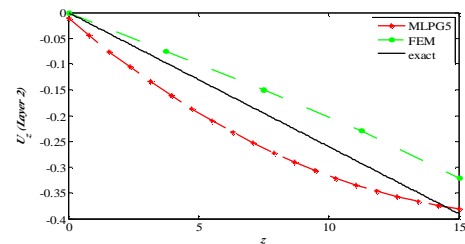


Figure 19. Lengthwise displacement diagram for the outer layer at $\theta = 45^\circ$ and $r = 6.5$ for the two-layer cylinder.

The three-dimensional node distribution of the MLPG5 model with 120 nodes, including 5 nodes in the radial, 3 nodes in the tangential and 8 nodes in the lengthwise direction is shown in Figure 13. Among them, 48 nodes are merely located in the inner layer, 48 ones are placed only in the outer layer, and the remaining 24 nodes lay on the interface. For FEM solution, by using software ANSYS, we have defined 16 elements and 162 nodes in meshing process with the same element type “SOLID95” (Figures 14 and 15). The material properties of each element were defined according to the layer in which that element was resided. The technique introduced in Section 4 is employed to deal with material discontinuity. Like the one-layer case, displacements and stresses are computed at $z = 7.5$ and $\theta = 45^\circ$ (Figures 16 to 18). Further, the lengthwise displacement of each layer is obtained at $\theta = 45^\circ$ and the average radiuses of second layer; i.e. $r = 6.5$ (Figure 19). The results are promising; specially, at the interface, which confirm the effectiveness of the proposed technique in comparison with finite element method. As shown in Figures 7 and 15, the number of nodes for the FEM are much less than the one-layer

cylinder; but its results are still fine and in radial displacement and radial stress diagrams (Figures 16 and 17) are almost better than MLPG5. This also implicates the convergence of FEM solution. However, in the Hoop stress diagram (Figure 18), at the material discontinuity boundary ($r = 5$), the ANSYS solution gives an average amount of stress between two true magnitudes. That's because of defining nodes exactly on the material boundary. As we know, FEM solution merely gives the results at nodes and since these nodes belong to both layers, the jumping Hoop stress magnitude has become an average of two true ones. Furthermore, it is noticeable that because the coding of the problem is very heavy and complicated, especially in the case of the numerical integration, the convergency of the obtained results didn't check for these problems. However, the authors, study the convergency of the proposed method for other problems, such as those of reported in [40-43].

6. CONCLUSION

The MLPG5 technique is applied for the analysis of the thick-walled laminated cylinders made from the isotropic materials under the elasto-static pressure. The elasto-static analysis of the thick-walled cylinders is a suitable examination for the three-dimensional application of the meshless methods. Due to the high continuity of the approximation functions, the material discontinuity is a serious difficulty in meshless methods. Since the MLPG method is conceptually one of the most attractive approaches; in this article, a simple technique embedding a sense of the domain decomposition is introduced to tackle the difficulty of the material discontinuity. In this technique, the nodes on the material boundaries have two integration domains, one in the lower layer and the other in the upper one, i.e. the problem domain is treated as a number of separate domains (depending on the number of material layers). Results are quite acceptable and promising; specially, at the material interface which demonstrate the efficiency of the proposed technique in comparison with the exact solutions and FEM results.

7. REFERENCES

1. Atluri, S. and Zhu, T., "A new meshless local petrov-galerkin (MLPG) approach in computational mechanics", *Computational Mechanics*, Vol. 22, No. 2, (1998), 117-127.
2. Chen, T. and Raju, I., "A coupled finite element and meshless local petrov-galerkin method for two-dimensional potential problems", *Computer Methods in Applied Mechanics and Engineering*, Vol. 192, No. 41, (2003), 4533-4550.
3. Xiao, J., "Local heaviside weighted mlpg meshless method for two-dimensional solids using compactly supported radial basis functions", *Computer Methods in Applied Mechanics and Engineering*, Vol. 193, No. 1, (2004), 117-138.
4. Qian, L., Batra, R. and Chen, L., "Static and dynamic deformations of thick functionally graded elastic plates by using higher-order shear and normal deformable plate theory and meshless local petrov-galerkin method", *Composites Part B: Engineering*, Vol. 35, No. 6, (2004), 685-697.
5. Li, Q., Soric, J., Jarak, T. and Atluri, S.N., "A locking-free meshless local petrov-galerkin formulation for thick and thin plates", *Journal of Computational Physics*, Vol. 208, No. 1, (2005), 116-133.
6. Ma, Q., "Meshless local petrov-galerkin method for two-dimensional nonlinear water wave problems", *Journal of Computational Physics*, Vol. 205, No. 2, (2005), 611-625.
7. Sladek, J., Sladek, V. and Zhang, C., "Stress analysis in anisotropic functionally graded materials by the mlpg method", *Engineering Analysis with Boundary Elements*, Vol. 29, No. 6, (2005), 597-609.
8. Ching, H. and Yen, S., "Meshless local petrov-galerkin analysis for 2d functionally graded elastic solids under mechanical and thermal loads", *Composites Part B: Engineering*, Vol. 36, No. 3, (2005), 223-240.
9. Batra, R.C., Porfiri, M. and Spinello, D., "Analysis of electrostatic mems using meshless local Petrov-Galerkin (MLPG) method", *Engineering Analysis with Boundary Elements*, Vol. 30, No. 11, (2006), 949-962.
10. Sladek, J., Sladek, V. and Hon, Y., "Inverse heat conduction problems by meshless local Petrov-Galerkin method", *Engineering Analysis with Boundary Elements*, Vol. 30, No. 8, (2006), 650-661.
11. Kaiyuan, L., Shuyao, L. and Guangyao, L., "A simple and less-costly meshless local petrov-galerkin (mlpg) method for the dynamic fracture problem", *Engineering Analysis with Boundary Elements*, Vol. 30, No. 1, (2006), 72-76.
12. Xiao, J., Batra, R., Gilhooley, D., Gillespie Jr, J. and McCarthy, M., "Analysis of thick plates by using a higher-order shear and normal deformable plate theory and mlpg method with radial basis functions", *Computer Methods in Applied Mechanics and Engineering*, Vol. 196, No. 4, (2007), 979-987.
13. Sladek, J., Sladek, V., Krivacek, J., Wen, P. and Zhang, C., "Meshless local petrov-galerkin (MLPG) method for reissner-mindlin plates under dynamic load", *Computer Methods in Applied Mechanics and Engineering*, Vol. 196, No. 25, (2007), 2681-2691.
14. Gilhooley, D., Batra, R., Xiao, J., McCarthy, M. and Gillespie Jr, J., "Analysis of thick functionally graded plates by using higher-order shear and normal deformable plate theory and mlpg method with radial basis functions", *Composite Structures*, Vol. 80, No. 4, (2007), 539-552.
15. Liu, L. and Tan, J., "Meshless local petrov-galerkin approach for coupled radiative and conductive heat transfer", *International Journal of Thermal Sciences*, Vol. 46, No. 7, (2007), 672-681.
16. Hu, D., Long, S., Han, X. and Li, G., "A meshless local petrov-galerkin method for large deformation contact analysis of elastomers", *Engineering Analysis with Boundary Elements*, Vol. 31, No. 7, (2007), 657-666.
17. Li, D., Lin, Z. and Li, S., "Numerical analysis of mindlin shell by meshless local Petrov-Galerkin method", *Acta Mechanica Solida Sinica*, Vol. 21, No. 2, (2008), 160-169.
18. Wu, X.-H. and Tao, W.-Q., "Meshless method based on the local weak-forms for steady-state heat conduction problems", *International Journal of Heat and Mass Transfer*, Vol. 51, No. 11, (2008), 3103-3112.
19. Gilhooley, D., Xiao, J., Batra, R., McCarthy, M. and Gillespie Jr, J., "Two-dimensional stress analysis of functionally graded solids using the mlpg method with radial basis functions", *Computational Materials Science*, Vol. 41, No. 4, (2008), 467-481.
20. Sladek, J., Sladek, V., Wen, P. and Hon, Y., "Inverse fracture problems in piezoelectric solids by local integral equation method", *Engineering Analysis with Boundary Elements*, Vol. 33, No. 8, (2009), 1089-1099.

21. Li, Y., Feng, W. and Xu, Z., "Fracture analysis of cracked 2d planar and axisymmetric problems of magneto-electro-elastic materials by the MLPG coupled with fem", *Computer Methods in Applied Mechanics and Engineering*, Vol. 198, No. 30, (2009), 2347-2359.
22. Sladek, J., Sladek, V., Sulek, P. and Zhang, C., "Fracture analysis in continuously nonhomogeneous magneto-electro-elastic solids under a thermal load by the mlpg", *International Journal of Solids and Structures*, Vol. 47, No. 10, (2010), 1381-1391.
23. Vaghefi, R., Baradaran, G. and Koohkan, H., "Three-dimensional static analysis of thick functionally graded plates by using meshless local petrov-galerkin (mlpg) method", *Engineering Analysis with Boundary Elements*, Vol. 34, No. 6, (2010), 564-573.
24. Wen, P., "Meshless local petrov-galerkin (MLPG) method for wave propagation in 3D poroelastic solids", *Engineering Analysis with Boundary Elements*, Vol. 34, No. 4, (2010), 315-323.
25. Wu, X.-H., Tao, W.-Q., Shen, S.-P. and Zhu, X.-W., "A stabilized mlpg method for steady state incompressible fluid flow simulation", *Journal of Computational Physics*, Vol. 229, No. 22, (2010), 8564-8577.
26. Rezaei Mojddehi, A., Darvizeh, A., Basti, A. and Rajabi, H., "Three dimensional static and dynamic analysis of thick functionally graded plates by the meshless local petrov-galerkin (MLPG) method", *Engineering Analysis with Boundary Elements*, Vol. 35, No. 11, (2011), 1168-1180.
27. Xia, P., Long, S. and Wei, K., "An analysis for the elasto-plastic problem of the moderately thick plate using the meshless local Petrov-Galerkin method", *Engineering Analysis with Boundary Elements*, Vol. 35, No. 7, (2011), 908-914.
28. Hosseini, S.M., Sladek, J. and Sladek, V., "Meshless local Petrov-Galerkin method for coupled thermoelasticity analysis of a functionally graded thick hollow cylinder", *Engineering Analysis with Boundary Elements*, Vol. 35, No. 6, (2011), 827-835.
29. Shibahara, M. and Atluri, S., "The meshless local petrov-galerkin method for the analysis of heat conduction due to a moving heat source, in welding", *International Journal of Thermal Sciences*, Vol. 50, No. 6, (2011), 984-992.
30. Mahmoodabadi, M., Abedzadeh Maafi, R., Bagheri, A. and Baradaran, G., "Meshless local Petrov-Galerkin method for 3D steady-state heat conduction problems", *Advances in Mechanical Engineering*, Vol. 2011, (2011).
31. Najafi, M., Arefmanesh, A. and Enjilela, V., "Meshless local Petrov-Galerkin method-higher reynolds numbers fluid flow applications", *Engineering Analysis with Boundary Elements*, Vol. 36, No. 11, (2012), 1671-1685.
32. Nikfar, M. and Mahmoodi, M., "Meshless local petrov-galerkin analysis of free convection of nanofluid in a cavity with wavy side walls", *Engineering Analysis with Boundary Elements*, Vol. 36, No. 3, (2012), 433-445.
33. Sladek, J., Sladek, V., Stanak, P., Zhang, C. and Wunsche, M., "Analysis of the bending of circular piezoelectric plates with functionally graded material properties by a mlpg method", *Engineering Structures*, Vol. 47, No., (2013), 81-89.
34. Arefmanesh, A., Najafi, M. and Musavi, S., "Buoyancy-driven fluid flow and heat transfer in a square cavity with a wavy baffle—meshless numerical analysis", *Engineering Analysis with Boundary Elements*, Vol. 37, No. 2, (2013), 366-382.
35. Atluri, S.N. and Shen, S., "The meshless local petrov-galerkin (mlpg) method, Crest, (2002).
36. Li, Q., Shen, S., Han, Z. and Atluri, S., "Application of meshless local Petrov-Galerkin (MLPG) to problems with singularities, and material discontinuities, in 3-D elasticity", *Computer Modeling in Engineering and Sciences*, Vol. 4, No. 5, (2003), 571-586.
37. Krongauz, Y. and Belytschko, T., "EFG approximation with discontinuous derivatives", *International Journal for Numerical Methods in Engineering*, Vol. 41, No. 7, (1998), 1215-1233.
38. Cordes, L. and Moran, B., "Treatment of material discontinuity in the element-free galerkin method", *Computer Methods in Applied Mechanics and Engineering*, Vol. 139, No. 1, (1996), 75-89.
39. Liu, G.-R. and Gu, Y.-T., "An introduction to meshfree methods and their programming, Springer, (2005).
40. Baradaran, G. and Mahmoodabadi, M., "Optimal pareto parametric analysis of two dimensional steady-state heat conduction problems by mlpg method", *International Journal of Engineering (IJE), Transactions B: Applications*, Vol. 22, No. 4, (2009), 387-406.
41. Baradaran, G.H. and Mahmoodabadi, M.J., "Parametric study of the mlpg method for the analysis of three dimensional steady state heat conduction problems", *Journal of Mechanical Engineering*, Vol. 61, No. 1, (2010), 31-61.
42. Baradaran, G., Mahmoodabadi, M. and Sarfarazi, M., "Analyze of 3D elasto-static problems by meshless local Petrov-Galerkin method", *International Journal of Advanced Design and Manufacturing Technology*, Vol. 3, No. 2, (2011), 37-44.
43. Bagheri, A., Ehsany, R., Mahmoodabadi, M. and Baradaran, G., "Optimization of meshless local Petrov-Galerkin parameters using genetic algorithm for 3d elasto-static problems (technical note)", *International Journal of Engineering-Transactions A: Basics*, Vol. 24, No. 2, (2011), 143-152.
44. Timoshenko, S., Goodier, J. and Abramson, H.N., "Theory of elasticity", Third Edition, McGraw-Hill, (1970).

Appendix A.

The Exact Elasto-Static Solutions for the Thick-Walled One-Layer Cylinder

Consider a thick-walled cylinder of the length L , internal radius r_i , and external radius r_o subjected to the uniform internal pressure p_i and external pressure p_o (Figure 16). We assume that it long enough so that the lengthwise strain ε_z is independent of the radius variable r . Because of axial symmetry and absence of shear loads, the tangential displacement and all of the shear stresses are zero. Axis Z is along the length of the cylinder and the material's behavior is assumed totally elastic. According to the boundary conditions, the radial and hoop stresses are [44]:

$$\text{B.C: } \begin{cases} \sigma_r = -p_i & \text{at } r = r_i \\ \sigma_r = -p_o & \text{at } r = r_o \end{cases} = \begin{cases} \sigma_r = \frac{p_i r_i^2 - p_o r_o^2}{r_o^2 - r_i^2} - \frac{(p_i - p_o) r_i^2 r_o^2}{r_o^2 - r_i^2} \left(\frac{1}{r^2}\right) \\ \sigma_\theta = \frac{p_i r_i^2 - p_o r_o^2}{r_o^2 - r_i^2} + \frac{(p_i - p_o) r_i^2 r_o^2}{r_o^2 - r_i^2} \left(\frac{1}{r^2}\right) \end{cases} \quad (\text{A-1})$$

If an axial effective force P is exerted to the cylinder in the closed-end case, thus the lengthwise stress will be:

$$\sigma_z = \begin{cases} 0 & \text{open - end} \\ \frac{P}{\pi(r_o^2 - r_i^2)} = \frac{p_i r_i^2}{r_o^2 - r_i^2} & \text{closed - end} \end{cases} \quad (\text{A-2})$$

To obtain the radial and lengthwise displacements, we should employ the stress-strain relations:

$$\begin{cases} \varepsilon_r = \frac{\partial u_r}{\partial r} = \frac{1}{E}(\sigma_r - \nu(\sigma_\theta + \sigma_z)) \\ \varepsilon_\theta = \frac{u_r}{r} = \frac{1}{E}(\sigma_\theta - \nu(\sigma_r + \sigma_z)) \\ \varepsilon_z = \frac{\partial u_z}{\partial z} = \frac{1}{E}(\sigma_z - \nu(\sigma_r + \sigma_\theta)) \end{cases} \quad (\text{A-3})$$

For the special case $p_o = 0$, the displacement values are as follows:

$$u_r = \frac{p_i r_i^2}{E} \left(\frac{a r + (1+\nu) r_i^2}{r(r_i^2 - r^2)} \right), \alpha = \begin{cases} 1 - \nu & \text{open - end} \\ 1 - 2\nu & \text{closed - end} \end{cases} \quad (A-4)$$

Appendix B.

The Exact Elasto-Static Solutions for the Thick-Walled Two-Layer Cylinder

Consider a two-layer thick-walled cylinder of the length L , internal radius a , middle radius b , and external radius c , subjected to uniform internal pressure p_i and external pressure p_o (Figure 17). We assume that the layers are placed freely beside each other and have no deflection before being pressed. Therefore, for each layer, we can use the one-layer cylinder relations with the equal conditions at the material interface, i.e. the radial displacement and radial stress should be the same at the middle radius $r = b$. Suppose the radial stress to be an unknown value p_m at $r = b$, then the hoop stress at this radius will be [44]:

$$\text{at } r = b \quad \sigma_{r_i} = \sigma_{r_o} = -p_m \Rightarrow \begin{cases} \sigma_{\theta_i} = \frac{p_i a^2 - p_m b^2}{b^2 - a^2} + \frac{(p_i - p_m) a^2}{b^2 - a^2} \\ \sigma_{\theta_o} = \frac{p_m b^2 - p_o c^2}{c^2 - b^2} + \frac{(p_m - p_o) c^2}{c^2 - b^2} \end{cases} \quad (B-1)$$

By applying the stress-tangential strain relation and imposing the displacement equality condition ($u_{r_i} =$

u_{r_o}), we can obtain the value of p_m in terms of the known parameters. Here, it has been evaluated only for the open-end case (regarding to the problems stated in section 5) and the other case is surrendered to readers.

$$p_m = \frac{E_o(2p_i a^2(c^2 - b^2)) + E_i(2p_o c^2(b^2 - a^2))}{E_o(c^2 - b^2)[b^2 + a^2 - \nu_i(b^2 - a^2)] + E_i(b^2 - a^2)[c^2 + b^2 + \nu_o(c^2 - b^2)]} \quad (B-2)$$

Eventually, the stresses and displacements can be obtained from the stress-strain relations, if each layer is considered as a separate cylinder.

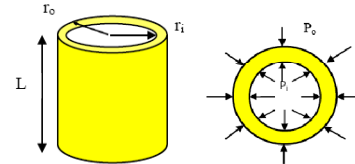


Figure 16. One-layer cylinder under pressure; prospective and cross section.



Figure 17. Two-layer cylinder under pressure; prospective and cross section.

Meshless Local Petrov-Galerkin Method for Elasto-Static Analysis of Thick-walled Isotropic Laminated Cylinders

M. J. Mahmoodabadi^a, M. M. Sarfarazi^b, A. Bagheri^b, G. H. Baradaran^c

^a Department of Mechanical Engineering, Sirjan University of Technology, Sirjan, Iran.

^b Department of Mechanical Engineering, University of Guilan, Rasht, Iran.

^c Department of Mechanical Engineering, Shahid Bahonar University, Kerman, Iran.

P A P E R I N F O

چکیده

Paper history:

Received 18 March 2014
 Received in revised form 15 April 2014
 Accepted 26 June 2014

Keywords:

Meshless Local Petrov-Galerkin (MLPG)
 Moving Least Squares (MLS)
 Material Discontinuity
 Thick-Walled Laminated Cylinders

در این مقاله یکی از معمول ترین و ساده ترین اعضای خانواده روشهای بدون المان پتروف - گالرکین محلی (MLPG) به نام MLPG5، جهت تحلیل مخازن استوانه ای جدار ضخیم لایه ای ایزوتروپیک تحت فشار الاستو-استاتیک به کار گرفته شده است. یک روش ساده جدید جهت رفع مشکل بسیار مهم روشهای بدون المان در مورد ناپیوستگی مواد به علت پیوستگی بالای توابع شکلشان پیشنهاد شده است. از تقریب حداقل مربعات بازگشتی جهت تشکیل توابع سعی و از تابع پله هویساید ساده برای توابع آزمون استفاده شده است. روش اعمال مستقیم جهت ارضای شرایط مرزی بکار گرفته شده است. تطابق قابل قبول نتایج با جوابهای تحلیلی و اجزا محدود به ویژه در مرزهای ناپیوسته ماده، حاکی از موفقیت روش پیشنهادی بوده و روش مذکور در حل سایر مسایل مقدار مرزی نیز توصیه می شود.

doi: 10.5829/idosi.ije.2014.27.11b.11